Carbon 116 (2017) 133–138

Contents lists available at ScienceDirect

Carbon

journal homepage: www.elsevier.com/locate/carbon

Fast growth of large single-crystalline graphene assisted by sequential double oxygen passivation

Jiewei Chen [a], Mengqi Cui [a], Gaoxiang Wu [a], Tianyue Wang [a], Joseph Michel Mbengue [a], Yingfeng Li [a], Meicheng Li [a, b, *]

[a] State Key Laboratory of Alternate Electrical Power System with Renewable Energy Sources, North China Electric Power University, Beijing, 102206, China
[b] Chongqing Materials Research Institute, Chongqing, 400707, China

ARTICLE INFO

Article history:
Received 7 November 2016
Received in revised form
12 January 2017
Accepted 31 January 2017
Available online 1 February 2017

Keywords:
Fast growth of larger single-crystal graphene
Sequential double oxygen passivation
Oxygen induced weak carbon adsorption energy

ABSTRACT

Graphene has been considered an extraordinary platform for electronic applications, while it still remains a challenge to fast synthesize large single-crystalline graphene (LSCG) for widespread use. Since the adsorption energy of single carbon on the substrate plays an important role in the nucleation and growth of graphene, we have considered adjusting its adsorption energy to synthesize LSCG. Here, our density functional theory (DFT) calculations expose that oxygen can significantly reduce (~1.03 eV) the adsorption energy of single carbon on oxygen-covered Cu compared with the bare Cu. Motivated by the calculation result that oxygen can induce weaker carbon adsorption energy, the sequential double oxygen passivation method through chemical vapor deposition is proposed to successfully grow the millimeter-scale single-crystalline graphene with the rate of about 100 μm min^{-1}. This approach could provide a new sight into fast synthesizing LSCG facilely and economically.

1. Introduction

Graphene is an ideal two-dimensional carbon material [1–4] with the combined properties of excellent mechanical [5,6], electrical [7] and optical properties [8], which has been widely used for various applications [9,10]. Compared to the low yield through mechanical exfoliation [11], graphene synthesized by chemical vapor deposition (CVD) is more effective for industrial-scale production [12], while it is concerning that the traditional CVD-grown graphene on Cu always exhibits a polycrystalline nature with weaker electrical properties [13]. At present, massively synthesis of large single-crystal graphene (LSCG) with the similar excellent properties to the exfoliated graphene [14] is significant for practical applications.

Tremendous efforts have been made to reduce the nucleation density to grow LSCG such as substrate pre-treating [15–18] and gas supply controlling [19–23]. Especially, oxygen introduction is proved effective for assisting LSCG growth, but its role during the synthesis process is still shrouded by mist. Actually, oxygen exhibits a crucial but mysterious role relying on the introducing ways: regarding the short-period oxygen passivation after annealing, the active nucleation sites can be passivated [24], and as for the continuous oxygen supply, hydrocarbon can be faster decomposed by lowering the energy barriers [25]. Moreover, it is reported that oxygen can act as other roles in reducing the nucleation density [26–30].

Beyond the nucleation density reduction, a high growth rate is also essential for massive synthesis [1,2]. The carbon-source supply is an important factor in controlling the growth of LSCG on Cu substrate [31]. Tianru Wu et al. reported the fast growth of inch-sized single-crystalline graphene by locally feeding carbon precursors to a desired position [1]. Subsequently, Zhongfan Liu et al. reported the fast growth of single-crystal graphene on Cu substrate through multistage carbon-source [14]. It is indicated that the carbon-source could play a mutually restricted role in the growth process of graphene: i.e., a lower carbon-source in the nucleation process can reduce the nucleation density, while the higher carbon-source in the growth process can promote the growth kinetics of graphene, which may also induce new nucleation [14,32].

Based on the unique roles of carbon-source supply and oxygen introduction in the reduction of nucleation density and acceleration of growth, a novel oxygen-assisted carbon-source supply

* Corresponding author. State Key Laboratory of Alternate Electrical Power System with Renewable Energy Sources, North China Electric Power University, Beijing, 102206, China.
E-mail address: mcli@ncepu.edu.cn (M. Li).

http://dx.doi.org/10.1016/j.carbon.2017.01.108
0008-6223/

strategy is proposed to fast grow LSCG on the Cu substrate. This strategy adopts a sequential double oxygen passivation method (SDOP): the first oxygen passivation during the nucleation process combined with low carbon supply can help reduce low nucleation density, and the second oxygen passivation combined with high carbon supply can enhance the growth rate.

2. Experiment and calculation

2.1. Growth and characterization of graphene

Large single-crystal graphene was grown using low pressure chemical vapor deposition (LPCVD). Here we apply a CVD system, using a quartz tube as the reaction chamber. Briefly, commercial copper foils (25-μm thick, 99.8%, polycrystalline, Alfa Aesar, #13382) were cleaned using isopropanol, acetone, and CH_3COOH. Afterwards, the quartz is used as the base to support the copper, and the copper is bended to wrap the quartz, as shown in Fig. S1a, and then is loaded into the CVD chamber, and placed at the center of the furnace. Then the system was vacuumed to approximately 1 Pa by a mechanical pump for 10 min before the tube was heated up to 1040 °C and anneal for some time. The first oxygen passivation was introduced in the nucleation process followed by the low supply of methane while the second oxygen passivation was introduced in the growth process followed by the high supply of methane. The O_2 supply in each process: about 0.1sccm lead to the vacuum of 2 Pa. The CH_4/H_2 supply ratio in nucleation process is 1:300 while the CH_4/H_2 supply in the growth process is 1:5. The detailed gas supply, reaction time and temperature can be seen in SI Fig. 2. The individual graphene domain was transferred onto SiO_2/Si substrates, using PMMA-assisted wet method for Raman characterizations. The individual graphene domain was also transferred to TEM grid for SAED with the help of PMMA and acetone.

The morphology was observed by FESEM (FEI Quanta 200F microscope field emission scanning electron microscope) and TEM (Tecnai G2 F20 Field emission transmission electron microscopy) with accelerating voltage of 200 kV. X-ray photoelectron spectrum (XPS) analysis was conducted with a ESCALAB 250Xi X-ray photoelectron spectroscope equipped with Al Kα radiation, and the binding energy was calibrated by the C1s peak (284.8 eV) of contaminated carbon. Raman spectra was investigated with the equipment Horiba Jobin Yvon(HJY) LabRAM. Time-of-flight secondary ion mass spectrometry (TOF-SIMS) was conducted using Cs+ for sputtering (45°).

2.2. Calculation details

All calculations were conducted using the DFT integrated in the Dmol^3 model in Materials Studio of Accelrys Inc. The double-z numerical basis set with polarization functions (DNP) and DFT semicore pseudopotential (DSPP) were used, and the electron exchange and correlation effects were described by the Perdew–Burker–Ernzerhof (PBE) method, a generalized gradient approximation (GGA)-type exchange–correlation function. During our calculations, the real-space cut off of a plane wave was set at 4.0 Å; the k-point mesh was set to 1 × 1 × 1; fermi smearing was adopted. The self-consistent-field (SCF) density convergence threshold value was set at 1×10^{-5} hartree.

The Cu (111) facet was simulated using a periodic 5-layer slab of 6 × 6 super cells, which contains 180 copper atoms. Repeated slabs are separated by about 10 Å vacuum to avoid interactions between neighboring slabs, and the final lattice parameters used are 15.336 Å × 15.336 Å × 18.348 Å.

The single carbon atom was imported to various sites on the Cu (111) surface and the geometry of the system was optimized with the aforementioned sets. The adsorption energies $E_{c-Cu\ ads}$ of per carbon atom here are defined as

$$E_{c-Cu\ ads} = E_{c+Cu\ surface} - E_{Cu\ surface} - E_c \quad (1)$$

where $E_{c+Cu\ surface}$ stands for the energy of a system having a carbon atom adsorbed on the copper surface, $E_{Cu\ surface}$ is the energy of a clear copper surface, and E_c is the energy of an isolated carbon atom under vacuum. With this definition, negative adsorption energies would be obtained, which correspond to the exothermic adsorption process.

The second system imports one layer of oxygen (12 oxygen atoms) on above Cu (111) facet. Then, single carbon atom was adsorbed on the oxygen covered Cu surface, and corresponding adsorption energy $E_{c-oxygen\ covered\ Cu\ ads}$, was calculated with the similar workflow to calculate $E_{c-Cu\ ads}$, as follows:

$$E_{c-oxygen\ covered\ Cu\ ads} = E_{c+Oxygen-covered\ surface} - E_{Oxygen-covered\ surface} - E_c \quad (2)$$

where $E_{Oxygen-covered\ surface}$ is the energy of oxygen covered copper surface, and E_c is the energy of an isolated carbon atom under vacuum.

3. Results and discussion

For hydrocarbon conversion to CVD-grown graphene on Cu, there are three key processes: the catalytic decomposition of hydrocarbon to form active carbon species, graphene nucleation, and the subsequent growth from the nuclei [14,17,33,34]. Many works reported that the adsorption energy of the activated carbon plays an important role in the nucleation and growth processes of graphene [35–37]. As mentioned earlier, the introduction of oxygen plays an important but mysterious role in synthesizing graphene, it is motivating to investigate whether oxygen takes effects resulting from the oxygen-induced change of the adsorption energy. The adsorption energies of the activated carbon on the oxygen adsorbed Cu and the bare Cu have been calculated respectively through density functional theory (DFT). The calculation results expose that oxygen can cause the distinct difference between the adsorption energy of single carbon on the oxygen adsorbed Cu and the bare Cu, as shown in Fig. 1.

The adsorption reaction of the activated carbon on copper (Fig. 1a)can be described as follow:

$$C_{activated} \xrightarrow{Cu} C_{adsorbed}\,(-5.17\ eV) \quad (3)$$

whereas the adsorption of the activated carbon on oxygen covered copper (Fig. 1b) through the surface reaction is

$$C_{activated} \xrightarrow{oxygen-covered\ Cu} C_{adsorbed}\,(-4.14\ eV) \quad (4)$$

Obviously, there is significant carbon adsorption energy reduction (of 1.03 eV). Since the oxygen can induce weak carbon adsorption, and the carbon adsorption energy plays an important role in growing graphene, we have tried to fine control the introduction of oxygen to affect the synthesizing graphene process for fast growing LSCG.

As is discussed before, oxygen can induce the distinct change of the carbon adsorption energy and the adsorption energy strongly affects the nucleation and growth processes of graphene, so it will work if the oxygen is introduced during the nucleation and growth processes. To present a facile way to massively synthesize graphene for practical applications, the introduction of oxygen has been

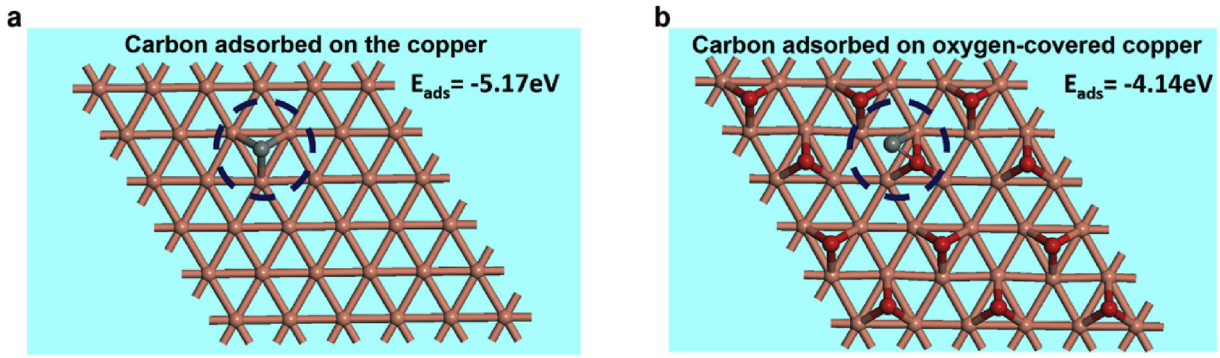

Fig. 1. The DFT calculations of the adsorption energy of single carbon on (a) bare copper and (b) oxygen covered copper. (A colour version of this figure can be viewed online.)

afforded just via the gas supply in CVD system. Since the carrier gas hydrogen may easily react with the oxygen, the oxygen is introduced earlier and the supply of carbon-source and hydrogen follows in each process. The affective factors in synthesizing graphene have been systematically investigated and after the fine control of the introduction of supply gas, the fast growth of LSCG has been achieved assisted by SODP (see synthesis details in SI Fig. 2).

The oxygen content in the Cu foil samples have been characterized and compared through TOF-SIMS as shown in SI Fig. 3. Similar to the OF-Cu in the TOF-SIMS reported by Hao et al. [24], the oxygen content of our Cu without oxygen passivation drops quickly when the depth varies from 0 to 200 nm. However, different from Cu without oxygen passivation and the reported work [24], the Cu after oxygen passivation shows a smooth decrease during 0–100 nm and then drops until 200 nm. When the depth exceeds 200 nm, the oxygen content in both samples maintains 10E-5 at. %.

Furthermore, we have used the XPS to characterize the chemical states of Cu (SI Fig. 4) and O (SI Fig. 5) in the surface of the copper. SI Fig. 4a shows that there only exists one peak at 932.6 eV for samples H-Cu and O-H-Cu, and this peak corresponds to the Cu $2p_{3/2}$ peak of Cu [38]. And there are two more peaks at 933.7 eV (CuO) [30], and at 934.7 eV ($Cu(OH)_2$) [38] for samples as-received Cu (SI Fig. 4b) and pretreated Cu (SI Fig. S4c). From Fig. S4, it can be concluded that: there is much $Cu(OH)_2$ and CuO in the native oxide surface of as-received Cu. Even after being pretreated by isopropanol, acetone, and CH_3COOH, there still remains high concentration of $Cu(OH)_2$ and CuO. After heating up and annealing under hydrogen, there is only Cu for the sample H-Cu because the $Cu(OH)_2$ and CuO can be reacted with hydrogen and transferred to Cu. After oxygen passivation, there is no obvious difference of XPS Cu 2p for the O-H-Cu compared to H-Cu, indicating that during the oxygen passivation, the reaction of transforming Cu to CuO or $Cu(OH)_2$ doesn't occur.

Meanwhile, we have investigated the high resolution XPS O1s characterization of these four samples, as shown in SI Fig. 5. Considering that there only exists pure Cu peak in H-Cu and O-H-Cu confirmed by high resolution XPS Cu 2p in SI Fig. 4, the XPS O1s curves of H-Cu and O-H-Cu can be divided into two peaks, 530.7 nm for adsorbed oxygen and 531.5 nm for hydroxyl/carbonate [39]. From SI Fig. 5b and c, it can be concluded that after oxygen passivation, the concentration of adsorbed oxygen (530.7 nm) increases much higher than that of hydroxyl/carbonate (531.5 nm). In addition, in the as-received Cu and pretreated Cu, for one thing, there are CuO and $Cu(OH)_2$ confirmed by high resolution XPS Cu 2p in SI Fig. 4, so there must be the relative oxygen peaks. For another, it's reported that there exist the surface organic contaminants [40],

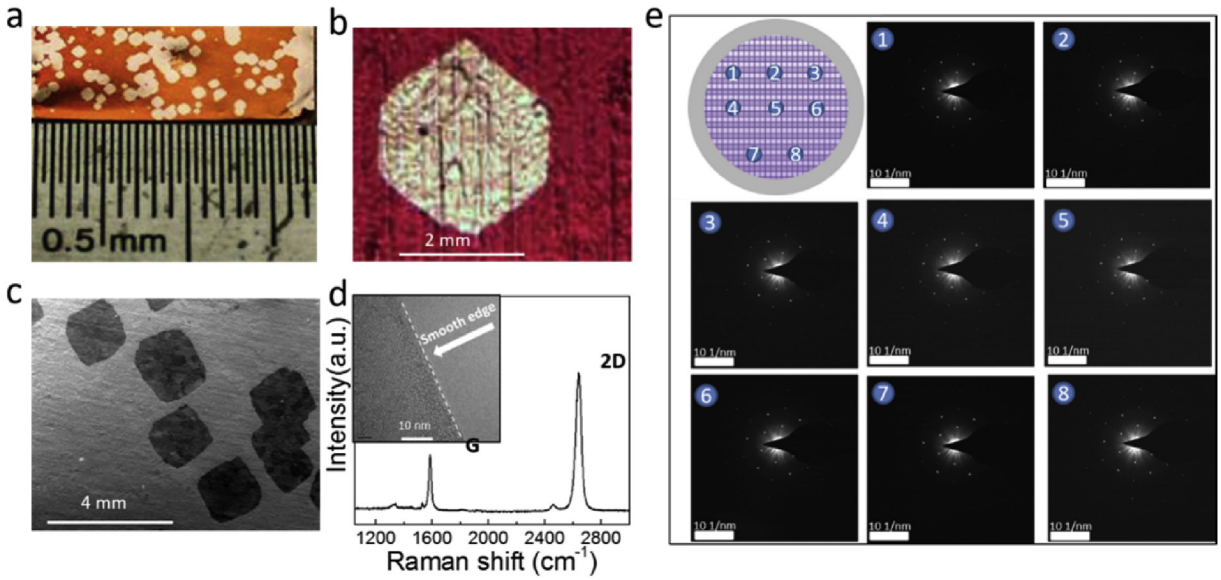

Fig. 2. Characterization of synthesized graphene. (a, b) Optical photograph and optical microscopy image of graphene on Cu foil after CVD and oxidation in air. (c) SEM image of graphene (d) Raman spectrum of graphene. Inset: the HRTEM image of graphene. (e) SAED characterization of synthesized graphene to demonstrate the single crystal of graphene. (A colour version of this figure can be viewed online.)

which consist of complicated oxygen peaks. Due to these two points, it is hard to divide the one large peak of CuO and $Cu(OH)_2$ into specific small peaks.

The synthesized LSCG has been characterized to reveal its properties, as shown in Fig. 2. Fig. 2a shows an optical photograph of synthesized graphene on a Cu foil. This sample was heated in air for 5 min at 200 °C to create a contrast between graphene-covered Cu and bare Cu, enabling us to clarify the size and morphology of graphene. It's obvious that the synthesized graphene is millimeter-scale (~2 mm), which is consistent with the optical microscopy image of prepared graphene shown in Fig. 2b and the SEM image of graphene in Fig. 2c. More importantly, the Raman spectra of prepared graphene shows that the ratio of 2D peak (2670 cm^{-1}) to G peak (1600 cm^{-1}) is higher than 2, which means that the synthesized graphene is monolayer [16,25], further supported by the HRTEM image of graphene edge (the inset in Fig. 2d). To demonstrate the single-crystal nature of the prepared graphene over millimeter scale, we transferred it to a TEM micro grid, and performed selected area electron diffraction (SAED), as shown in Fig. 2e. Eight different sites were randomly selected in the transferred flake, only a suit of hexagonal diffraction spots with negligible rotation was noticed, indicating that selected area is a single crystalline flake [41,42]. Thus, the fast growth of LSCG can be efficiently achieved assisted by SDOP.

To clarify the mechanism of SDOP on the fast synthesis of LSCG, first oxygen passivation during nucleation and second oxygen passivation growth has been investigated respectively to indicate their effects on synthesizing graphene, as is shown in Fig. 3. Obviously, there are less flakes and larger graphene about 2 mm (Fig. 3a) when O_2 is introduced in these processes, and the growth

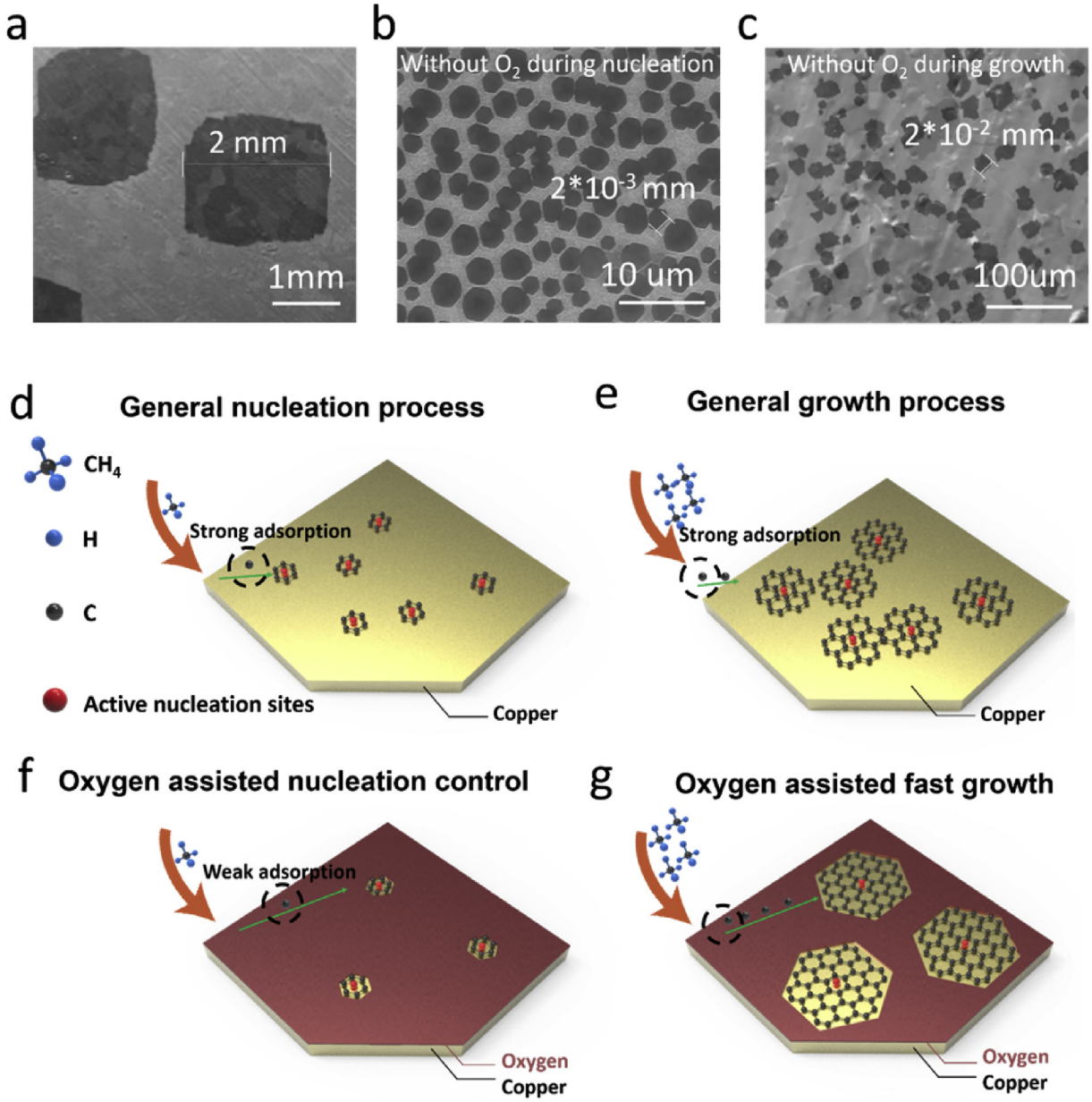

Fig. 3. Effects of O_2 adsorption during nucleation and growth on the synthesis of graphene. The SEM images of the growth graphene (a) with the O_2 during both nucleation and growth processes (b) without the O_2 during nucleation process, and (c) without the O_2 during growth process. (d, e) The traditional nucleation and growth of graphene. (f, g) Sequential double oxygen passivation (SDOP) assisted nucleation and growth of graphene. (A colour version of this figure can be viewed online.)

rate reaches up to 100 μm min^{-1}.

On the nucleation process, after the first oxygen passivation, the relatively low concentration of CH_4 is introduced to form the nucleation, as illustrated in Fig. 3f. When no oxygen is introduced in the nucleation, the nucleation density (as shown in Fig. 3b) is much higher than that in Fig. 3a, which means that the oxygen can help decrease the nucleation density.

The effects of adsorbed oxygen on controlling the nucleation of graphene are explained by the oxygen induced weak carbon adsorption affecting mechanism. Based on our DFT calculations, there is a significant difference (1.03 eV reduction) between the adsorption energy of single carbon on oxygen adsorbed Cu and bare Cu. The significant adsorption energy reduction can hinder the activated carbon atom to be adsorbed to the oxygen covered copper and thus will help decrease the nucleation density of graphene. This mechanism is consistent with our experimental observation (Fig. 3) that the first oxygen passivation can help control the nucleation density combined with the relatively low supply of carbon source. Thus, the introduced first oxygen passivation in our work can play an active role in controlling the nucleation of graphene for growing LSCG based on the oxygen-induced weak adsorption.

On the growth process, we apply the oxygen to secondly adsorb the surface of Cu before the relatively high concentration of CH_4 is introduced to grow graphene, as illustrated in Fig. 3g. When O_2 is not introduced at this stage, the single-crystal graphene grows to about 0.2 mm (Fig. 3c). But still, in the same reaction time, they are smaller and the nucleation density is higher than graphene (~2 mm) in Fig. 3a. Thus, in addition to decreasing graphene nucleation density, O also affected the graphene growth rate. Importantly, it should be emphasized that since higher concentration of H_2 in the nucleation process may easily react with and eliminate adsorbed oxygen on the copper, it's necessary to apply the second oxygen passivation to ensure the rich oxygen adsorbed on the copper for oxygen assisted fast growth of LSCG. The growth size of graphene at different times can be seen in SI Fig. 6, which shows that the average growth rate of graphene is about 100 μm min^{-1}.

Since the fast growth of LSGC can be attributed to the highly active carbon flux which can promote the reaction kinetics between the graphene nuclei and the activated carbon [25,43], it is expected that the second oxygen passivation plays an active role in enhancing active carbon supply. To prove this assumption, we have investigated the effects of the adsorption energy on the carbon flux. The adsorption energy can be described as

$$E_{ads} = E_{c+surface} - E_{surface} - E_c \quad (5)$$

which is an exothermic reaction process [44,45], so the stronger adsorption energy can lead to more stable adsorption of the activated carbon. Hence, due to the weaker adsorption and its relative reduced energy barrier (1.03 eV) of the carbon on the oxygen-covered Cu according to our DFT calculations, it is much easier for the carbon to desorb and diffuse from the surface of oxygen-covered Cu and thus will greatly increase the flux of active carbon. Therefore, during the growth process, in addition to hindering the new nucleation sites of graphene, oxygen induced weak carbon adsorption can also promote the graphene growth rate.

What's more, we have investigated the effects of different oxygen pressures on the growth of graphene. From SI Fig. 7, it can be concluded that as the oxygen flow rate increases from 1, 1.5, 2 to 2.5 Pa, the size of the graphene becomes less rectangular and more hexagonal. A little different from the reported works [46–49], the changing law of the growth shape is not really consistent with the reported works as the oxygen flow rate increases. It is assumed that this result can be attributed to the two reasons: firstly, the growth rate of graphene can enhanced due to the effects of oxygen induced low adsorption energy of the single carbon confirmed by our theory calculation and experiments. Secondly, the effects of etching by oxygen as reported by many works. Hence, combined with our DFT calculations and experimental phenomena, it implies that the oxygen induced weak carbon adsorption mechanism can assist in lowering the nucleation density and promoting the growth kinetics. Considering this point with the well-established reported roles of oxygen [24,25], the fast growth of LSCG assisted by SDOP can be explained.

4. Conclusions

In conclusion, we have demonstrated a novel carbon-source supply strategy to fast synthesize LSCG on Cu substrate assisted by SDOP. First oxygen passivation during the nucleation combined with low carbon supply enables the formation of low nucleation density, while the second oxygen passivation during the growth process combined with high carbon supply can greatly enhance the growth rate of the graphene grown on Cu substrate. Basically, the fast growth of LSCG results from the oxygen induced weak carbon absorption and its cooperative effects of low nuclear density and fast growth rate. With the assistance of SDOP, the millimeter-scale single-crystalline graphene grows at a speed up to 100 μm min^{-1}. This approach could be helpful in promoting the development of synthesizing LSCG more facilely and economically.

Acknowledgements

This work is supported partially by National High-tech R&D Program of China (863 Program, No. 2015AA034601), National Natural Science Foundation of China (Grant nos. 91333122, 51372082, 51402106 and 11504107), Ph.D. Programs Foundation of Ministry of Education of China (Grant nos. 20130036110012), Par-Eu Scholars Program, Beijing Municipal Science and Technology Project (Z161100002616039) and the Fundamental Research Funds for the Central Universities (2016JQ01, 2015ZZD03, 2015ZD07).

Appendix A. Supplementary data

Supplementary data related to this article can be found at http://dx.doi.org/10.1016/j.carbon.2017.01.108.

References

[1] T. Wu, et al., Fast growth of inch-sized single-crystalline graphene from a controlled single nucleus on Cu-Ni alloys, Nat. Mater 15 (2016) 43–47.
[2] X. Li, et al., Synthesis of graphene films on copper foils by chemical vapor deposition, Adv. Mater 28 (2016) 6247–6252.
[3] D. Geng, et al., Graphene single crystals: size and morphology engineering, Adv. Mater 27 (2015) 2821–2837.
[4] Z. Chen, et al., Fast and uniform growth of graphene glass using confined-flow chemical vapor deposition and its unique applications, Nano Res. (2016) 1–8.
[5] K. Min, et al., Mechanical properties of graphene under shear deformation, Appl. Phys. Lett. 98 (2011), 013113–013113-013113.
[6] C. Lee, et al., Measurement of the elastic properties and intrinsic strength of monolayer graphene, Science 321 (2008) 385–388.
[7] Z.S. Wu, et al., Synthesis of graphene sheets with high electrical conductivity and good thermal stability by hydrogen arc discharge exfoliation, Acs Nano 3 (2009) 411–417.
[8] K.F. Mak, et al., Measurement of the optical conductivity of graphene, Phys. Rev. Lett. 101 (2008) 6797–6800.
[9] T. Mueller, et al., Graphene photodetectors for high-speed optical communications, Nat. Photonics 4 (2010) 297–301.
[10] X. Li, et al., Synthesis of graphene films on copper foils by chemical vapor deposition, Adv. Mater 28 (2016) 6247–6252.
[11] K.S. Novoselov, et al., Electric field effect in atomically thin carbon films, Science 306 (2004) 666–669.
[12] C.W. Huang, et al., Observing the evolution of graphene layers at high current density, Nano Res. (2016) 1–8.
[13] Z. Yan, et al., Correction to toward the synthesis of wafer-scale single-crystal graphene on copper foils, Acs Nano 6 (2012) 9110–9117.

[14] L. Lin, et al., Rapid growth of large single-crystalline graphene via second passivation and multistage carbon supply, Adv. Mater 28 (2016) 4671–4677.
[15] H. Zhou, et al., Chemical vapour deposition growth of large single crystals of monolayer and bilayer graphene, Nat. Commun. 4 (2013) 2096.
[16] M.-C. Chuang, et al., Nucleation and growth dynamics of graphene on oxygen exposed copper substrate, Carbon 103 (2016) 384–390.
[17] J. Kraus, et al., Suppressing graphene nucleation during CVD on polycrystalline Cu by controlling the carbon content of the support foils, Carbon 96 (2016) 153–165.
[18] Q. Li, et al., Controllable seeding of single crystal graphene islands from graphene oxide flakes, Carbon 79 (2014) 406–412.
[19] R. Gulotty, et al., Effect of hydrogen flow during cooling phase to achieve uniform and repeatable growth of bilayer graphene on copper foils over large area, Carbon 77 (2014) 341–350.
[20] Y. Hao, et al., Oxygen-activated growth and bandgap tunability of large single-crystal bilayer graphene, Nat. Nanotechnol. 11 (2016) 426–431.
[21] X. Li, et al., Graphene films with large domain size by a two-step chemical vapor deposition process, Nano Lett. 10 (2010) 4328–4334.
[22] X. Li, et al., Large-area graphene single crystals grown by low-pressure chemical vapor deposition of methane on copper, J. Am. Chem. Soc. 133 (2011) 2816–2819.
[23] L. Gan, et al., Turning off hydrogen to realize seeded growth of subcentimeter single-crystal graphene grains on copper, ACS Nano 7 (2013) 9480–9488.
[24] Y. Hao, et al., The role of surface oxygen in the growth of large single-crystal graphene on copper, Science 342 (2013) 720–723.
[25] X. Xu, et al., Ultrafast growth of single-crystal graphene assisted by a continuous oxygen supply, Nat. Nanotechnol. 11 (2016) 930–935.
[26] J. Pang, et al., Oxidation as A Means to remove surface contaminants on Cu foil prior to graphene growth by chemical vapor deposition, J. Phys. Chem. C 119 (2015).
[27] G. Eres, et al., Cooperative island growth of large-area single-crystal graphene on copper using chemical vapor deposition, Acs Nano 8 (2014) 5657–5669.
[28] C.C. Chen, et al., Growth of large-area graphene single crystals in confined reaction space with diffusion-driven chemical vapor deposition, Chem. Mater 27 (2015).
[29] S. Gottardi, et al., Comparing graphene growth on Cu(111) versus oxidized Cu(111), Nano Lett. 15 (2015) 917–922.
[30] M.C. Chuang, et al., Nucleation and growth dynamics of graphene on oxygen exposed copper substrate, Carbon 103 (2016) 384–390.
[31] K. Yan, et al., Designed CVD growth of graphene via process engineering, Acc. Chem. Res. 46 (2013) 2263–2274.
[32] Z. Yan, et al., Chemical vapor deposition of graphene single crystals, Acc. Chem. Res. 47 (2014) 1327–1337.
[33] X. Li, et al., Large-area synthesis of high-quality and uniform graphene films on copper foils, Science 324 (2009) 1312–1314.
[34] Y. Li, et al., An important atomic process in the CVD growth of graphene: sinking and up-floating of carbon atom on copper surface, Appl. Surf. Sci. 284 (2013) 207–213.
[35] X. Li, et al., Evolution of graphene growth on Ni and Cu by carbon isotope labeling, Nano Lett. 9 (2009) 4268–4272.
[36] C. Hwang, et al., Initial stage of graphene growth on a Cu substrate, J. Phys. Chem. C 115 (2011) 22369–22374.
[37] H.I. Rasool, et al., Continuity of graphene on polycrystalline copper, Nano Lett. 11 (2010) 251–256.
[38] C. Jia, et al., Direct optical characterization of graphene growth and domains on growth substrates, Sci. Rep. 2 (2011), 707–707.
[39] K. Sutthiumporn, et al., Promotional effect of alkaline earth over Ni–La 2 O 3 catalyst for CO 2 reforming of CH 4 : role of surface oxygen species on H 2 production and carbon suppression, Fuel Energy Abstr. 36 (2011) 14435–14446.
[40] J. Pang, et al., Oxidation as A Means to remove surface contaminants on Cu foil prior to graphene growth by chemical vapor deposition, J. Phys. Chem. C 119 (2015), 150601131157001.
[41] Z. H, et al., Chemical vapour deposition growth of large single crystals of monolayer and bilayer graphene, Nat. Commun. 4 (2013) 131–140.
[42] X. Chen, et al., Chemical vapor deposition growth of 5 mm hexagonal single-crystal graphene from ethanol, Carbon 94 (2015) 810–815.
[43] Y. Li, et al., DFT study on the atomic-scale nucleation path of graphene growth on the Cu(111) surface, Phys. Chem. Chem. Phys. Pccp 16 (2014) 5213–5220.
[44] F. Callevallejo, et al., Introducing structural sensitivity into adsorption-energy scaling relations by means of coordination numbers, Nat. Chem. 7 (2015).
[45] P. Koskinen, et al., Self-passivating edge reconstructions of graphene, Phys. Rev. Lett. 101 (2008) 6037–6040.
[46] S. Choubak, et al., Graphene CVD: interplay between growth and etching on morphology and stacking by hydrogen and oxidizing impurities, J. Phys. Chem. C 118 (2014) 21532–21540.
[47] X. Chen, et al., Chemical vapor deposition growth of 5 mm hexagonal single-crystal graphene from ethanol, Carbon (2015) 810–815.
[48] E. Starodub, et al., Oxidation of graphene on metals, J. Phys. Chem. C 114 (2010) 5134–5140.
[49] L. Lin, et al., Rapid growth of large single-crystalline graphene via second passivation and multistage carbon supply, Adv. Mater 28 (2016) 4671–4677.